Icarus 221 (2012) 289–295

Contents lists available at SciVerse ScienceDirect

Icarus

journal homepage: www.elsevier.com/locate/icarus

Locations of thin liquid water layers on present-day Mars

Akos Kereszturi [a,b,*], Edgard G. Rivera-Valentin [c]

[a] Konkoly Observatory, Research Centre for Astronomy and Earth Sciences, Hungarian Academy of Sciences, H-1121 Budapest, Konkoly Thege M. 15-17, Hungary
[b] New Europe School for Theoretical Biology and Ecology, H-1038 Budapest, Hollos Korvin 5, Hungary
[c] Department of Geological Sciences, Brown University, 324 Brook St., Box 1846, Providence, RI 02912, United States

ARTICLE INFO

Article history:
Received 18 January 2012
Revised 2 August 2012
Accepted 3 August 2012
Available online 14 August 2012

Keywords:
Mars
Exobiology
Ices
Mars, surface
Mars, polar caps

ABSTRACT

CRISM indicates the presence of water ice patches in Richardson crater, located on Mars' southern polar region at the area of the seasonal ice cap. Numerical simulations suggest that the maximum daytime temperature of the ice at these locations is between 195 and 220 K during local spring. Previous studies suggest that at these temperatures liquid interfacial water could be present. Here, for the first time, we provide an example where the environmental conditions allow for the formation of such liquid films on present day Mars at the southern hemisphere. The upper bound estimated H_2O loss during the presence of these water ice patches is approximately 30 μm between Ls = 200 and 220, though it may be as low as 0.1 μm depending on the ambient water vapor. The upper bound value is larger than the expected condensation thickness in autumn; however, it may still be realistic due to CO_2 gas jet generated deposition and possible subsequent accumulation on mineral grains. The presence of this interfacial water may have impact on local chemical processes along with astrobiological importance.

1. Introduction

The mounting evidence that liquid water is present on Mars today is one of the most important regarding active geochemical processes and the planet's astrobiological potential. Some theoretical models predict that liquid water may be present (Clow, 1987; Haberle et al., 2001; Hecht, 2002), above all as interfacial water (Mohlmann, 2004, 2010; Kossacki and Markiewicz, 2008) where water ice is in physical contact with mineral grains. Salts may influence the appearance of liquid water by decreasing the melting point. The presence of brines is suggested by the observations at the Phoenix landing site and other locations (Kossacki et al., 2004a,b; Chevrier et al., 2009; Hecht et al., 2009; Renno et al., 2009), which may act as a possible agent for the formation of some recent flow-like features (Brass, 1980; Mellon and Phillips, 2001; Knauth and Burt, 2002; Motazedian, 2003; Kossacki et al., 2004a,b) at polar dunes too (Kereszturi et al., 2009; Szynkiewicz et al., 2009) – although dry mass movements could also produce these (Hansen et al., 2010).

In this study, we analyze one special type of location where brines and interfacial water are possible on Mars, the Dark Dune Spots. These spots, which we abbreviate as DDS (Horvath et al., 2001), are part of the great number of interesting seasonal features that appear during local spring in the polar regions of Mars. Larger spots in this group contain a water ice layer on their ring-shaped outer area (Kereszturi et al., 2011) surrounding the darkest and barren central core. In this ring-like feature, the surface is darker than the CO_2 ice covering surrounding terrains and as a result it absorbs more sunlight and thus experiences higher temperatures than the bright frost. Temperature measurements of the martian surface are available with spatial resolution substantially worse than the diameter of these spots (50–100 m). Since the temperature during the presence of water ice cover may be close to the threshold limit (180 K) for interfacial water formation along the mineral–water ice interface, it is important to elucidate the possible appearance of liquid interfacial water at the DDS. In this study, we modeled the temperature at these small areas in order to investigate the possibility of liquid water formation.

2. Methods

Observational data and modeling results were used to analyze the possibility of interfacial water at the target regions. Imaging data was acquired from the Mars Reconnaissance Orbiter (MRO) High Resolution Imaging Science Experiment (HiRISE), and topographic data from MOLA and HRSC digital terrain models (DTMs) based on stereo images.

2.1. Observational data analysis

Using CAT-ENVI software (Morgan et al., 2009), we analyzed CRISM spectral data (Murchie et al., 2007) within Richardson crater

* Corresponding author at: Konkoly Observatory, Research Centre for Astronomy and Earth Sciences, Hungarian Academy of Sciences, H-1121 Budapest, Konkoly Thege M. 15-17, Hungary.
E-mail address: kereszturi.akos@csfk.mta.hu (A. Kereszturi).

0019-1035/$ - see front matter © 2012 Elsevier Inc. All rights reserved.
http://dx.doi.org/10.1016/j.icarus.2012.08.004

(72°S179°E) using CRISM "FRT" observations (Full Resolution Targeted), which are characterized by a high spatial and spectral resolution (18 m and 7 nm respectively). Near-IR wavelengths were considered between 1 and 4 μm, observations were corrected for photometry and atmospheric gas absorptions (McGuire et al., 2009), and a filtering method (Parente, 2008) is used to reduce noise. The interpretation of spectra measured by push-broom sensors may be influenced by the effect called "spectral smile": the mean wavelength of spectels (spectel is the contents of a spectral channel for a particular pixel) and the spectral resolution can slightly change from one spatial pixel to the next (Ceamanos and Douté, 2009). We do not correct for the spectral smile because we take spectra near the center of the CRISM image where band shifts are lower than 0.002 μm (McGuire et al., 2009), which has a minor impact on wide and deep absorption bands.

For the albedo measurements, HiRISE images were also used and the gained results were correlated to TES based albedo estimations in order to have more than one source of information – although the worse spatial resolution TES data made possible was used only to correlate the trends in albedo changes. Absolute albedo values were approximated from HiRISE images using the *DN* values of certain pixels from the RED channel images. We calculated the reflectivity with the formula $I/F = (DN * \text{SCALING\_FACTOR}) + \text{OFFSET}$, and divided it with $\cos i$, in order to have approximated Lambertian albedo, which shows the same radiance when viewed from any angle. The Lambertian albedo is a good approximation of the albedo of the ice covered surface of Richardson crater at this time of the year. The resulting value, though, depends on several factors, such as the surface roughness, and especially on the incidence angle used in the correction. Although small-scale topography might affect the observed and calculated albedo values, such small-scale topography on Mars is unknown and cannot be taken into account – the used averages are the best approaches available. Beyond this theoretical argumentation the comparison between TES based measured and model based calculated values in this study (see Section 4) suggest that our model for the temperature estimation is realistic. We assume the terrain is a horizontal plane and also made several control measurements at various points of the analyzed "penumbra-like" area of the spots where water ice is covering the surface.

Albedo values were calculated and averaged for small 10×10 m square shaped homogeneous sections of the analyzed ring-like features. These sections were located manually, as rarely do small CO_2 patches appear at the ring-like or the barren central dark part. Based on manual analysis, the derived average albedo values are representative of the ring-like structure. The measured albedo values were scattered between 0.23 and 0.26 and on average 0.25. The TES based albedo values were also analyzed to validate and correlate the HiRISE based values and their changes. Unfortunately, TES data's spatial resolution is far worse than what is required for the analysis of structures as small as the ring-features. The correlation of HiRISE and TES based albedo values showed parallel trend, validating the analyzed albedo changes, but because of the low spatial resolution of TES data, HiRISE values were used for the model calculations in this study.

Temperature data was obtained from two sources: measured values with low spatial resolution (for comparison) and modeled values with high spatial resolution (for detailed analysis), where the latter could account for the small size of the target features. Observed values were derived from the Thermal Emission Spectrometer (TES) (MGS) measurements (Christensen et al., 1992), with "vanilla" software. This command line software is produced by the Arizona State University for the planetary science community to read and query binary data from TES dataset, correlate between various data tables, and was used presently to acquire surface temperature values for daytime between 12 and 14 local true solar time with spatial resolution of approximately 3–8 km. As a result, these values can only be considered a rough approximation of the surface temperature throughout the analyzed terrains and therefore are used only to analyze annual trends and to correlate them with model estimated values. For the analysis of certain solar longitude intervals at the surveyed locations, Thermal Emission Imaging System (THEMIS) and OMEGA (Visible and Infrared Mineralogical Mapping Spectrometer) data are not sufficient because their rare acquisition date and different local time.

2.2. Thermal modeling

Surface and subsurface temperatures were calculated by solving the one-dimensional thermal diffusion equation using a finite element approach as described by Rivera-Valentin et al. (2011), Rivera-Valentin (2012) and Ulrich et al. (2010). This method allows for the high spatial resolution required within this study. The vertical extent of the homogenous regolith column modeled was considered down to several times the annual skin depth in order to accurately reach convergence. Thus, the model simulated temperatures to a depth of 10 m with finite element thickness of 0.01 m and a corresponding time step of 10 s. The surface boundary condition for the column was considered radiative where the incoming solar heat flux is given by:

$$Q_{solar} = (1-A)\frac{S_0}{r^2}\cos\zeta T(\zeta,\tau) \tag{1}$$

where A is albedo, S_0 is the solar flux at 1 AU, r is the instantaneous Sun–martian distance in AU, ζ is the solar angle to zenith, and $T(\zeta, \tau)$ is the transmission coefficient, which is a function of the zenith angle and the atmospheric opacity (τ). As is shown in Blackburn et al. (2009), the transmission coefficient is a polynomial fit to the data from Pollack et al. (1990) as presented by Rapp (2008). Atmospheric perturbations to the incoming heat flux considered were the indirect solar illumination due to scattering ($Q_{scattering}$) and atmospheric thermal emission (Q_{IR}):

$$Q_{scattering} = (1-A)\frac{S_0}{r^2}(1-T(\zeta,\tau))f_{scat} \tag{2}$$

$$Q_{IR} = (1-A)\frac{S_0}{r^2}f_{atm}\varepsilon\cos(\delta-\phi) \tag{3}$$

where f_{scat} (0.02) and f_{atm} (0.04) are the fractional amounts of the relevant flux reaching the martian surface (Schmidt et al., 2009), δ is the solar declination, and ϕ is latitude (Kieffer et al., 1977; Applebaum and Flood, 1989; Aharonson and Schorghofer, 2006; Blackburn et al., 2009; Schmidt et al., 2009; Rivera-Valentin et al., 2010; Ulrich et al., 2010; Rivera-Valentin, 2012). The lower boundary condition includes a modest geothermal heat flux from below assigned as 30 mW/m^2 as previously applied by Ulrich et al. (2010).

We assumed a homogenous regolith column whose thermal properties were obtained as a weighted mass fraction of water ice and soil such that:

$$k = k_{ice}f_{ice} + k_{soil}(1-f_{ice}) \tag{4}$$

$$C = C_{ice}f_{ice} + C_{soil}(1-f_{ice}) \tag{5}$$

where k is thermal conductivity, C is volumetric heat capacity, f_{ice} is the fractional amount of ice within the soil column, and the subscripts denote the material. The thermal conductivity of water ice at the average surface temperature at the latitude considered is 3.4 W m^{-1} K^{-1} (Petrenko and Whitworth, 1999) with a volumetric heat capacity of 1.4×10^6 J m^{-3} K^{-1} (Giaque and Stout, 1936). The soil's thermal properties were obtained from the Phoenix Lander results, which found a thermal conductivity of 0.085 W m^{-1} K^{-1} and volumetric heat capacity of 1.05×10^6 J m^{-3} K^{-1} (Zent et al., 2010). We assumed a column composed of 60% mineral grains and 40% ice (i.e. $f = 0.4$) as this ratio is characteristic to regular sand supported material, and the voids there could be totally filled by late autumn H_2O condensation. In this case the total thermal conductivity of the modeled column is 1.4 W m^{-1} K^{-1} and volumetric heat capacity is 1.2×10^6 J m^{-3} K^{-1} with a corresponding thermal inertia of 1296 J m^{-2} K^{-1} $s^{-1/2}$. Thermal properties of the regolith column were considered constant throughout the simulation. The model was run for several martian years and considered to be converged to a static phase when the maximum temperature difference between the midnight temperature with depth profiles at the vernal equinox (Ls = 0) from two consecutive runs was less than 1 K. Using HiRISE and CRISM data together, we focused on the H_2O ice covered ring feature where no CO_2 ice is present and water ice cover was in direct contact with the surface of the mineral grains during the period between Ls = 200 and 220.

Modeled surface temperatures were used to estimate sublimation rates, which were calculated at every simulated time step. Sublimation of surface water ice under martian conditions has been shown to be well modeled by the Ingersoll equation (Sears and Chittenden, 2005; Chevrier and Altheide, 2008; Altheide et al., 2009), which is given by:

$$J_{Ing} = 0.17 D_{H_2O/CO_2} \Delta\eta \left[\frac{\left(\frac{\Delta\rho}{\rho}\right) g}{\upsilon^2}\right]^{\frac{1}{3}} \tag{6}$$

where D_{H_2O/CO_2} is the diffusivity of H_2O through the CO_2 atmosphere, $\Delta\eta$ is the water vapor density gradient between the surface and the atmosphere, $\Delta\rho$ is the surface to atmosphere relative density difference, g is gravity, and υ is the kinematic viscosity of CO_2 (Ingersoll, 1970; Taylor et al., 2006). Following the example of Ingersoll (1970), a dry atmosphere was assumed throughout the simulation and condensation was not considered; however, in order to examine the effect of atmospheric water vapor, we also considered water vapor a free variable. The values for atmospheric water vapor considered other than 0 Pa were 0.2 Pa and 1.5 Pa, which were obtained from the Phoenix Lander results (Zent et al., 2010, 2012). Though both a diurnal and seasonal variation on atmospheric water vapor is expected, constant water vapor is assumed and a range of possible values is studied in order to quantify its effect. Evaporative cooling caused by the sublimation of water ice was considered at every time step such that the total surface energy balance is given by:

$$Q_{total} = Q_{sun} + Q_{scattering} + Q_{IR} - \varepsilon\sigma T^4 - \rho \frac{dz}{dt} \Delta H_{sub} \tag{7}$$

where ε is emissivity, assumed here to be 0.95 (Kreslavsky and Head, 2005; Ulrich et al., 2010), σ is Stefan–Boltzman's constant, ρ is the density of ice, dz/dt is the instantaneous change in ice thickness, and ΔH_{sub} is the enthalpy of sublimation. The saturation vapor pressure of water ice was obtained from the extended formulation of Feistel and Wagner (2007).

3. Results

In this section, we first present evidence for the presence of a thin water ice layer in the outer ring-like area of the spots in Richardson crater. We then provide model-based estimates on the surface temperature inside these ring-like features. Modeling data is necessary to have temperature values where other datasets do not have high enough resolution.

3.1. Observations

Using CRISM and HiRISE data, a thin surface water ice cover was identified in the outer "penumbra" or ring-like structures in the Dark Dune Spots of Richardson crater (Fig. 1). Kereszturi et al. (2011) provide a detailed description of these features and the spatial and temporal behavior of water ice there. Using a series of CRISM images between Ls 175.5° and Ls 340.5° of Richardson crater, it can be noted that within the area of ring features, the bright CO_2 ice layer that surrounds the spots is missing. The thick wintertime deposited CO_2 ice cast shadows under low solar elevation for areas that are already defrosted. The thickness of CO_2 ice next to defrosted areas was estimated using the length of the shadow of the CO_2 layer and simple geometric calculations (details with graphics can be found at Kereszturi et al. (2011)). Based on shadow length measurements conducted relative to the top of the surrounding bright CO_2 ice cover, a horizontal depression about 10 cm deep is present at the ring-features. These depressions did not exist in earlier images, suggesting they formed due to localized sublimation of the CO_2 ice layer. By correlating CRISM based spectral data with HiRISE based optical images, a ~10 cm thick CO_2 ice layer is present on the terrain surrounding the spots while on the area of outer ring features only a thin (thinner than the 10 cm thick CO_2) H_2O ice layer is found (Figs. 2 and 3), and no ice is present within the darkest central core of spots, except for small frost patches at a few locations. For more details on the spectral identification of surface H_2O ice and its separation from the effect of atmospheric clouds, see Kereszturi et al. (2011).

3.2. Modeling

Using the aforementioned values and methods, the calculated annual temperature curve is compared to the TES based observed values for model validation, as illustrated in Fig. 3. The following

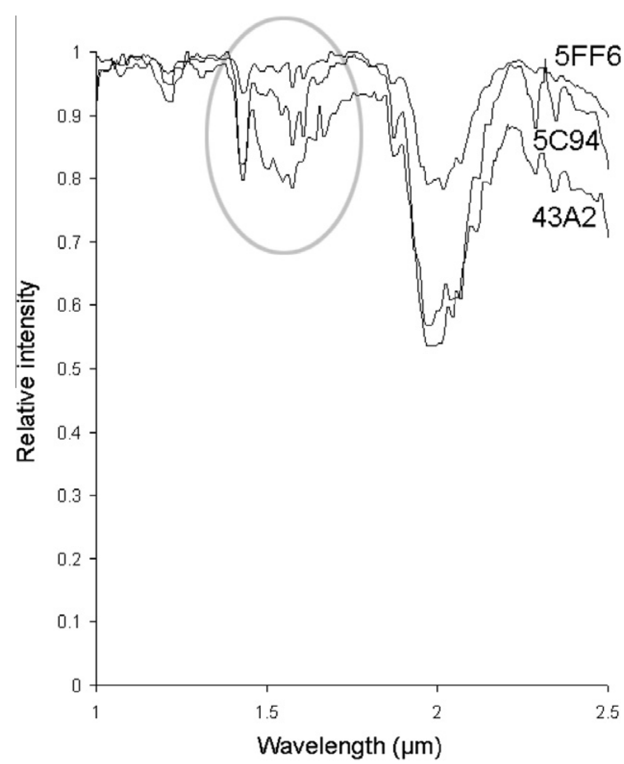

Fig. 1. Temporal change of water absorption band at 1.5 µm on CRISM images 43a2, 5C94, 5FF6 at Ls = 181.7, 242.7, 248.7 for the gray ring feature, normalized to the continuum, between 1.0 and 2.6 µm.

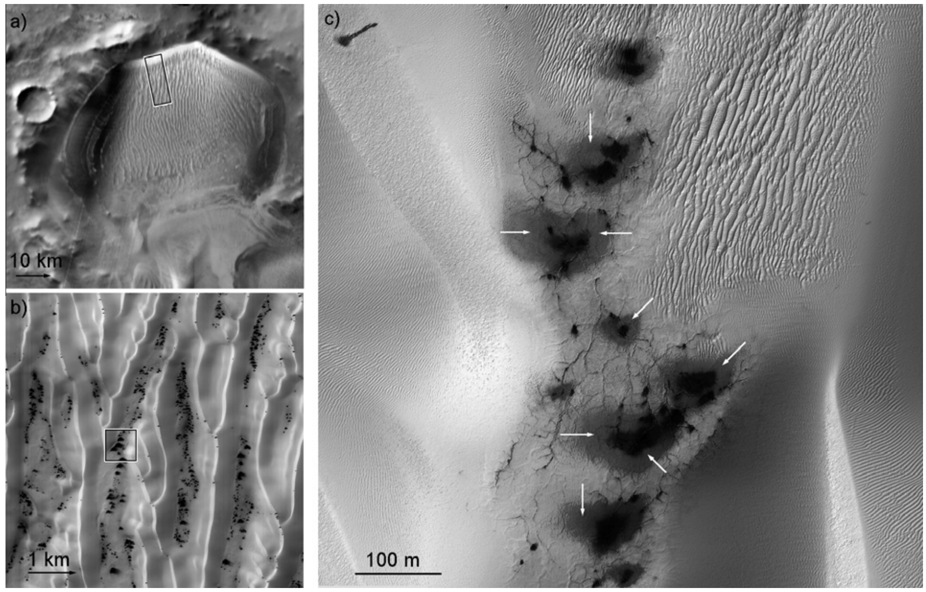

Fig. 2. Richardson crater (a) and a section of the HiRISE image PSP_002885_1080 (Ls = 197.01) (b), and its magnified part (c) with some spots where water ice covers the outer, here gray colored section (white arrows) where we modeled temperature variations.

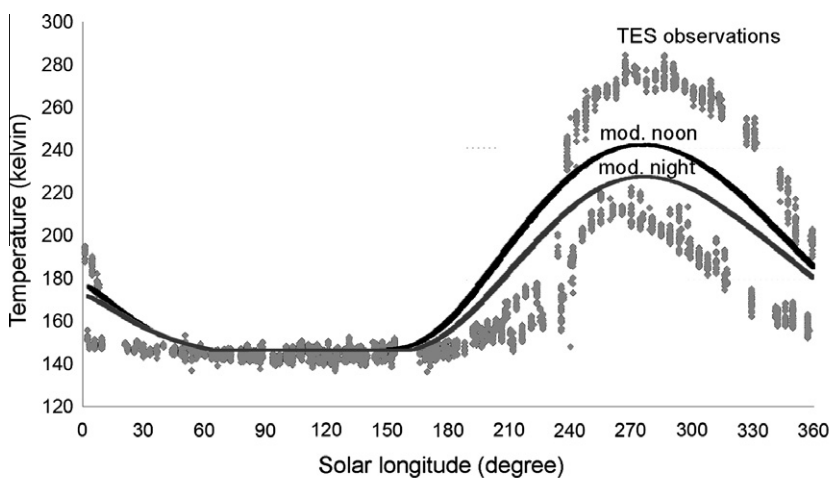

Fig. 3. Annual curves of TES based temperature observations (dotted) and modeled (mod.) daytime (black) and nighttime (gray) curves according to different solar longitudes (seasons) indicated along the horizontal axis. Daytime and nighttime curves differ from each other except the wintertime constant temperature phase (left), when continuous darkness was present. The letters mark the different sections of temporal changes, described in the text.

characteristics are visible in the image (letters are indicated to describe the phase and features of the curve in the text):

- On the left part of Fig. 3 (wintertime) nearly constant temperature values are observed on Mars (between a1 and a2), where the temperature is at the possible minimal value around the frost point of the atmospheric CO_2. Here only one modeled and one observed curve is present, as there is nearly constant temperature all along the martian sol. Modeled and observed curves overlap here, showing that the model well describes observations during this time.
- TES based curves start rising around Ls = 160–170 (b), marking the start of CO_2 defrosting when only small patches and not the whole terrain becomes free of CO_2 ice. Between Ls = 160 and 230 the temperature rises slowly. During this time (b2–b3), some part of the terrain is still covered and others are exhumed regarding the presence of CO_2 ice, but H_2O is still present.
- The CO_2 ice cover also starts to decrease around Ls = 160 in the model during daytime, while it may recondense onto the surface at nighttime till Ls = 170 (c1–c2). In the model, the wintertime CO_2 cover disappeared suddenly from all of the analyzed terrain as we used homogeneous surface, while in reality, due to inhomogenities, there are more CO_2 ice patches left behind for an extended period, causing the temperature to increase more slowly.
- Between Ls = 200 and 220, the modeled curve suggests higher temperatures than those observed (d1–d2). This is because the model only simulates the temperature of H_2O ice on the surface, while in the case of the observations (because of the low spatial resolution) cold CO_2 ice was also in the field of view of the detectors, thus lowering the average temperature for each pixel.
- Around Ls = 225–230 (e1–e2) the observed TES curve starts rising more rapidly, which may be due to water ice disappearing from below the already sublimated CO_2 ice cover.

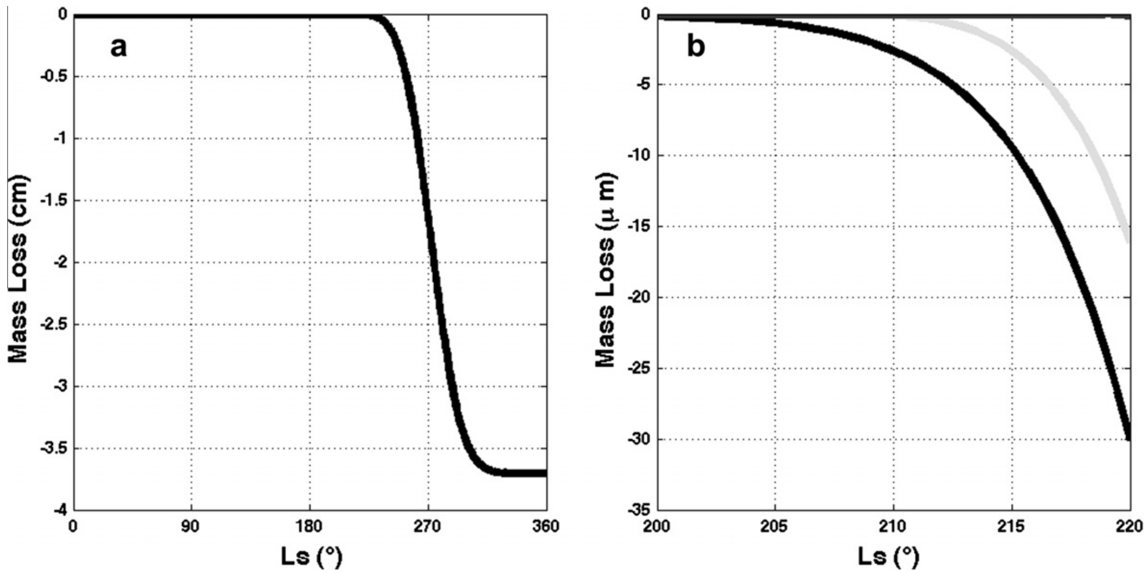

Fig. 4. The model based change of H_2O ice height according to solar longitude (a) and the magnified section (b) of the analyzed period for the studied constant atmospheric water vapor values with different shades of gray. The left panel shows the loss of "infinitely" thick water ice layer. In reality, though, the total earlier deposited H_2O ice might have been lost around Ls = 225–230.

- The summertime peak temperature is higher in the observed than the modeled case, since the model assumes constant ice cover (taken to be "infinite" water ice thickness) all along the period. Also, the albedo is higher than the barren dunes, and its sublimation also cools the surface.
- The amplitude of the modeled diurnal temperature cycle is smaller than the TES based observed fluctuation in summertime, as is expected based on theoretical argumentation. In our model, the water ice stays on the surface even in summertime (we have "endless thickness" of water ice and it cannot be totally lost by sublimation). As the thermal inertia of water ice is larger than the dry regolith, the summertime temperature amplitude will be much smaller than observations.

Errors in simulating surface temperature lie primarily in the assumption of a constant water ice layer and the estimates for albedo. The comparison of observed temperature data versus our simulated results clearly demonstrate the errors that arise from assuming a constant water ice layer. The temperature amplitude during summer is much lower than observed since the surface thermal inertia during this time within the model is much higher than in reality. Albedo values found ranged between 0.23 and 0.26 with an average of 0.25, which was assumed within the model. Application of these maximum and minimum albedo values to our model would shift the simulated maximum temperature to a range of 246–249 K, with the maximum predicted temperature using the average albedo being 247 K.

Beyond the temperature values, we estimated the net loss of the H_2O ice layer at the analyzed location, taking infinite thickness for the starting condition. A complete analysis of the effect of atmospheric water vapor on the sublimation rate requires a model of the diurnal variation of the planetary boundary layer (Zent et al., 1993). At night, when the planetary boundary layer (PBL) is at its thinnest, local relative humidity can reach saturation and thus sublimation rates will be hindered and condensation can occur. For simplicity, though, a constant value for atmospheric water vapor was assumed within the model and condensation was not accounted for. Most of the mass loss will occur during daytime when both high temperatures and a thick PBL are experienced. Sublimation rates were found for every modeled time step and summed in order to find the total amount of mass loss throughout the model. Fig. 4 shows the sublimation driven height loss in units of thickness for every Ls for the studied atmospheric water vapor values. Most of the ice sublimation occurs after Ls 180 when the southern hemisphere enters spring.

The graphs in Fig. 4 depict the running total net loss of water ice thickness. The daily loss of height at the beginning of the analyzed period at Ls 200 is about 1 μm/sol, while around the end at Ls 220 is around 4 μm/sol. Using the calculated sublimation rate during the whole observed presence of the water ice ring feature in the spots (Ls = 200–220), the total H_2O thickness that has been lost is around 30 μm, assuming a dry atmospheric column. The left curve works with assuming "infinite" water ice thickness, while in reality there is no more water ice cover on the surface after about Ls = 225.

The effect of atmospheric water vapor is to reduce the sublimation rate by decreasing the concentration gradient between the surface and atmosphere. As can be seen from Fig. 4, predicted sublimation rates for the relevant time period decreases from 30 μm assuming a dry atmosphere to 0.1 μm assuming 1.5 Pa of atmospheric water vapor. The true value may fall in between these results, as it would incorporate the diurnal and seasonal variation of atmospheric water vapor. The revised Phoenix Lander data suggests that the near-surface atmospheric water vapor remains at 0.17 Pa for most of the day, decreasing to 0.05 Pa at night (Zent et al., 2012; Rivera-Valentin, 2012) – although the interpretation of TECP data is somewhat uncertain. Since for an atmospheric water vapor value of 0.2 Pa, the sublimation rate was 16 μm, the true value may indeed be larger than the expected condensation thickness during autumn.

There are various uncertainties and simplifications in our model approach. The atmospheric water vapor is poorly known, and the exact ratio of the water ice and mineral grains embedded is also unknown and as a result there are uncertainties in the used bulk thermal coefficients. The albedo used is also an approximation from available observations. Despite these points, interpreting the modeled curves together with the observations and theoretical argumentation, the estimated temperature values may be realistic.

4. Discussion

4.1. Water ice at the Dark Dune Spots

Based on the CRISM and HiRISE data, a ring shaped H_2O ice layer is present on the surface at some so-called Dark Dune Spots in Richardson crater between Ls = 200 and 220, corresponding to about 38 martian sols. Here CO_2 ice in the surrounding and water ice in the ring-like area of the spots was identified by spectral data and confirmed by optical images (see details in Kereszturi et al. (2011)). Using modeled surface temperature values, the temperature on the water ice covered surface could reach 195–220 K during the "warmest" part of the day in this period. Analyzing the sublimation loss, we find that a predicted maximum of 30 μm of ice is lost between the period of Ls = 200 and 220. This implies for our observations that a layer approximately 30 μm thick may have been present on the surface at the beginning of the sublimation period, otherwise the water ice layer would have disappeared earlier.

The estimated 30 μm value is higher than the average 10 precipitable micrometer characteristic for the martian atmosphere, but cold trapping could produce such a thickness collecting H_2O continuously from the atmosphere as virtually any atmospheric circulation will deliver greater than unit atmospheric vapor column to a local cold trap. For example, it is possible that inhomogeneous ice condensation happens in autumn because of inhomogenities in the thermodynamic properties of the surface material, and/or local meteorological effects (winds, shadows of surrounding heights, etc.). Elevated water ice thickness might also be produced at theses spots by the CO_2 jet activity blowing up and depositing the water ice covered grains at the ring-like area of the spot during an earlier phase, increasing the local H_2O mass there. The observations suggest that the total ice mass at the observed locations disappears around this late date from the surface, while in greater depth there still may be intergranular ice, as it is suggested by thermal inertia and neutron spectrometric measurements.

4.2. Possible liquid at the Dark Dune Spots

It is interesting to analyze the theoretical possibility of liquid interfacial water along the ice–mineral boundary at the observed locations. Based on theoretical computations and laboratory observations, a quasi-liquid thin film exists at the interface that is kept in liquid phase mainly by Van-der-Waals forces (Mohlmann, 2004) above a threshold temperature. The exact temperature value depends on how much the minerals are in contact with water ice, and if there are salts embedded in the ice. Assuming pure H_2O ice, more than one monolayer thick liquid film exists above ~180 K (Mohlmann, 2004, 2008).

Using the model based temperature values, the minimum (nighttime) and maximum (daytime) values at the top of the insolated ice layer at the beginning of the observed period (Ls = 200) are 178 and 195 K respectively, while at the end of the ice presence (Ls = 220) these values are 200 and 220 K respectively. During this period, liquid interfacial water may indeed be present. In the case there exists other mechanisms to depress the melting point (e.g. salts), bulk brines may even be present. Taking the often cited Mars relevant ferric sulfate at a concentration of C = 48%, the melting point of water is depressed to 205 ± 1 K (Pestova et al., 2005; Chevrier and Altheide, 2008; Renno et al., 2009). Perchlorates were also found to be present at the landing site of Phoenix, which might decrease the melting point, in the case of 52 wt.% sodium perchlorate the eutectic point is 236 K, in the case of 44 wt.% of magnesium perchlorate the melting point is around 206 K (Chevrier et al., 2009). These arguments suggest that in the presence of salts, liquid brines might be present at the locations observed in this work. Though analysis of CRISM data did not demonstrate a liquid water signature in our earlier work (Mohlmann, 2008), we cannot rule out the presence of brines.

5. Conclusions

Analyzing the water ice covered ring-shaped area of the Dark Dune Spots at 72°S latitude, using accepted average martian atmospheric vapor concentration during the period of Ls = 200–220, the surface ice can reach the maximum daytime temperature between 195 and 220 K. This value is above the threshold limit where liquid interfacial water forms at the ice–mineral interface. Several earlier theoretical considerations (Zent et al., 1993; Mohlmann, 2004, 2010) showed that interfacial water may be on the martian surface. It is shown here for the first time that, at least in Richardson crater, there exists the proper environmental conditions for interfacial water. The thin interfacial layer may be present around the dune grains embedded in the top ice layer of the ring structure. Although the southern hemisphere of Mars is dryer than the northern hemisphere, based on the observations of water ice made here, a thin interfacial layer of liquid water may be present ephemerally.

The total simulated ice thickness that has been lost in this period is around 30 μm. This value is larger than the expected thickness by homogeneous atmospheric condensation, but it is realistic since in early spring, CO_2 gas driven jet activity may cover mineral grains with water ice at these ring structures.

Based on the observations and theoretical argumentation, the following structures and sequence of events may be relevant for the surface layer of the analyzed dunes in this springtime period: The basaltic grains plus fallen atmospheric dust could be cemented together with H_2O ice formed during autumn. This layer formed by direct condensation from the atmosphere during autumn and possibly by falling and accumulating ice crystals or snowflakes, as was observed by the Phoenix Lander (Smith et al., 2009). Later, CO_2 deposited on the surface and the whole terrain cooled down substantially. During springtime, when stronger insolation begins in the region, CO_2 gas-jets shoot dark dust above the ice layer. Later a gray ring forms around the center of the outburst, partly by this solar heated dark dust, which lowers the albedo. CO_2 ice then sublimates away and a thin H_2O ice covered surface layer is left behind. At the modeled temperature values, a thin layer of interfacial water or brine may be present at the mineral–ice interface for the warmer hours of a day, while the ice cover is still there. Based on our observations this may last for about 38 sols.

These liquid phases may have impact on the chemical and weathering processes and could also contribute to the formation of flow-like features (Mohlmann and Kereszturi, 2010) emanating from neighboring smaller spots, although dry mass movements may also produce them (Hansen et al., 2010). In this work, we have identified an important period at the analyzed latitude band and at small surface locations where focused analysis might give more information on the prospect of liquid water on Mars. Even though the northern martian hemisphere is water rich, the southern hemisphere has been shown to also be important for the occurrence of water ice and liquid water. In the search for the ideal location of bulk brine formation on Mars, these thin liquid water layers might provide example sites. These sites are also ideal for the identification of recent water-related alteration on Mars. The presence of liquids proposed in this study may even have biological implications at the DDS (Szathmary et al., 2007), though a more sophisticated model including the solid state greenhouse effect and the subsurface ice would be required for a biological investigation.

Acknowledgments

This study was supported by the ESA ECS Project No. 98076 (Co 4000105405) and the OTKA PD 105970 by the Hungarian Academy of Sciences. The authors would also like to thank the reviewers who helped enhance this manuscript.

References

Aharonson, O., Schorghofer, N., 2006. Subsurface ice on Mars with rough topography. J. Geophys. Res. 111, E11007.

Altheide, T., Chevrier, V., Nicholson, C., Denson, J., 2009. Experimental investigation of the stability and evaporation of sulfate and chloride brines on Mars. Earth Planet. Sci. Lett. 282, 69–78.

Applebaum, J., Flood, D. J., 1989. Solar radiation on Mars. Report No. NASA TM-102299.

Blackburn, D.G., Bryson, K.L., Chevrier, V.F., Roe, L.A., White, K.F., 2009. Sublimation kinetics of CO_2 ice on Mars. Planet. Space Sci. 58, 780–791.

Brass, G.W., 1980. Stability of brines on Mars. Icarus 42, 20–28.

Ceamanos, X., Douté, S., 2009. Spectral smile correction in CRISM hyperspectral images. AGU (Fall Meet.).

Chevrier, V.F., Altheide, T., 2008. Low temperature aqueous ferric sulfate solutions on the surface of Mars. Geophys. Res. Lett. 35, L22101.

Chevrier, V.F., Hanley, J., Altheide, T.S., 2009. Stability of perchlorate hydrates and their liquid solutions at the Phoenix landing site, Mars. Geophys. Res. Lett. 36, LXXXXX. http://dx.doi.org/10.1029/2009GL037497.

Christensen, P.R. et al., 1992. Thermal Emission Spectrometer experiment: Mars Observer mission. J. Geophys. Res. 97 (E5), 7719–7734.

Clow, G.D., 1987. Generation of liquid water on Mars through the melting of a dusty snowpack. Icarus 72, 95–127.

Feistel, R., Wagner, W., 2007. Sublimation pressure and sublimation enthalpy of H_2O ice Ih between 0 and 273.16 K. Geochim. Cosmochim. Acta 71, 36–45.

Giaque, W.F., Stout, J.W., 1936. The entropy of water and the third law of thermodynamics. The heat capacity of ice from 15 to 273 K. J. Am. Chem. Soc. 58, 1144–1150.

Haberle, R.M. et al., 2001. On the possibility of liquid water on present-day Mars. J. Geophys. Res. 106 (E10), 23317–23326.

Hansen, C.J., Thomas, N., Portyankina, G., McEwen, A., Becker, T., Byrne, S., Herkenhoff, K., Kieffer, H., Mellon, M., 2010. HiRISE observations of gas sublimation-driven activity in Mars' southern polar regions: I. Erosion of the surface. Icarus 205, 283–295.

Hecht, M.H., 2002. Metastability of liquid water on Mars. Icarus 156, 373–386.

Hecht, M.H. et al., 2009. Perchlorate in martian soil: Evidence and implications. Lunar Planet. Sci. 40. Abstract 2420.

Horvath, A., Ganti, T., Gesztesi, A., Berczi, Sz., Szathmary, E., 2001. Probable evidences of recent biological activity on Mars: Appearance and growing of Dark Dune Spots in the south polar region. Lunar Planet. Sci. 32. Abstract 1543.

Ingersoll, A.P., 1970. Mars: Occurrence of liquid water. Science 168, 972–973.

Kereszturi, A., Möhlmann, D., Berczi, Sz., Ganti, T., Kuti, A., Sik, A., Horvath, A., 2009. Recent rheologic processes on dark polar dunes of Mars: Driven by interfacial water? Icarus 201, 492–503.

Kereszturi, A., Vincendon, M., Schmidt, F., 2011. Water ice in the Dark Dune Spots of Richardson crater on Mars. Planet. Space Sci. 59, 26–42.

Kieffer, H.H., Martin, T.Z., Peterfreund, A.R., Jakosky, B.M., Miner, E.D., Palluconi, F.D., 1977. Thermal and albedo mapping of Mars during the Viking primary mission. J. Geophys. Res. 82, 4249–4291.

Knauth, L.P., Burt, D.M., 2002. Eutectic brines on Mars: Origin and possible relation to young seepage features. Icarus 158, 267–271.

Kossacki, K.J., Markiewicz, W.J., 2008. Martian hill-gullies, surface and sub-surface moisture. In: Mars Water Cycle Workshop, Paris.

Kossacki, K.J., Markiewicz, W.J., Wojciech, J., 2004a. Interfacial liquid water on Mars and its potential role in formation of hill and dune gullies. Icarus 210, 81–94.

Kossacki, K.J., Markiewicz, W.J., Wojciech, J., 2004b. Seasonal melting of surface water ice condensing in martian gullies. Icarus 171, 272–283.

Kreslavsky, M.A., Head, J.W., 2005. Mars at very low obliquity: Atmospheric collapse and the fate of volatiles. Geophys. Res. Lett. 32, L12202.

McGuire, P.C. et al., 2009. An improvement to the volcano-scan algorithm for atmospheric correction of CRISM and OMEGA spectral data. Planet. Space Sci. 57, 809–815.

Mellon, M.T., Phillips, R.J., 2001. Recent gullies on Mars and the source of liquid water. J. Geophys. Res. 106 (E10), 23165–23179.

Mohlmann, D., 2004. Water in the upper martian surface at mid- and low-latitudes: Presence, state, and consequences. Icarus 168, 318–323.

Mohlmann, D., 2008. The influence of van der Waals forces on the state of water in the shallow subsurface of Mars. Icarus 195, 131–139.

Mohlmann, D., 2010. The three types of liquid water in the surface of present Mars. Int. J. Astrobiol. 9, 45–49.

Mohlmann, D., Kereszturi, A., 2010. Viscous liquid film flow on dune slopes of Mars. Icarus 207, 654–658.

Morgan, F., Seelos, F., Murchie, S. 2009. CAT Tutorial, Presentation at the CRISM Workshop, The Woodlands, TX.

Motazedian, T., 2003. Currently flowing water on Mars. Lunar Planet. Sci. 34. Abstract 1840.

Murchie, S. et al., 2007. Compact Reconnaissance Imaging Spectrometer for Mars (CRISM) on Mars Reconnaissance Orbiter (MRO). J. Geophys. Res. 112, E05S03.

Parente, M., 2008. A new approach to denoising CRISM images. Lunar Planet. Sci. 39. Abstract 2528.

Pestova, O.N., Myund, L.A., Khripun, M.K., Prigaro, A.V., 2005. Polythermal study of the systems $M(ClO_4)_2–H_2O$ ($M^{2+} = Mg^{2+}$, Ca^{2+}, Sr^{2+}, Ba^{2+}). Russ. J. Appl. Chem. Engl. Transl. 78, 409–413.

Petrenko, V.F., Whitworth, R.W., 1999. Physics of Ice. Oxford University Press, New York.

Pollack, J.B., Haberle, R.M., Murphy, J.R., Schaeffer, J., Lee, H., 1990. Simulations of the general circulation of the martian atmosphere. I – Polar processes. J. Geophys. Res. 95, 1447–1473.

Rapp, D., 2008. Human Missions to Mars: Enabling Technologies for Exploring the Red Planet. Praxis Publishing, Chichester, UK.

Renno, N.O. et al., 2009. Physical and thermodynamical evidence for liquid water on Mars. Lunar Planet. Sci. 40. Abstract 1440.

Rivera-Valentin, E.G., 2012. Modeling H_2O Stability and Transport on Mars and Iapetus: Exploring Their Effects on Geomorphic and Atmospheric Processes. Ph.D. Dissertation, University of Arkansas, Fayetteville, AR.

Rivera-Valentin, E.G., Ulrich, R., Chevrier, V.F., Altheide, T.S., Wray, J.J., 2010. Dynamic modeling of maritan paleolake stability. Lunar Planet. Sci. Conf. Abstract #1446.

Rivera-Valentin, E.G., Blackburn, D.G., Ulrich, R., 2011. Revisiting the thermal inertia of Iapetus: Clues to the thickness of the dark material. Icarus 216, 347–358.

Schmidt, F., Doute, S., Schmitt, B., Vincendon, M., Bibring, J.P., Langevin, Y., Team, T.O., 2009. Albedo control of seasonal South Polar cap recession on Mars. Icarus 200, 374–394.

Sears, D.W.G., Chittenden, J.D., 2005. On laboratory simulation and the temperature dependence of the evaporation rate of brine on Mars. Geophys. Res. Lett. 32, 1–4.

Smith, P.H. et al., 2009. H_2O at the Phoenix landing site. Science 325, 58–61.

Szathmary, E. et al., 2007. Life in the Dark Dune Spots of Mars: A testable hypothesis. In: Pudritz, R., Higgs, P., Stone, J. (Eds.), Planetary Systems and the Origin of Life. Cambridge University Press, pp. 259–282.

Szynkiewicz, A., Ewing, R.C., Fishbaugh, K.E., Bourke, M.C., Bustos, D., Pratt, L.M., 2009. Geomorphological evidence of plausible water activity and evaporitic deposition in interdune areas of the gypsum-rich Olympia Undae dune field. Lunar Planet. Sci. 40. Abstract 2038.

Taylor, P., Baibakov, K., Brown, S., Hecht, M., Hudson, T., Li, P., Lange, C., Prieto, L., Savelyev, S., 2006. On the sublimation of ice particles on the surface of Mars; with applications to the 2007/8 Phoenix Scout mission. Icarus 181, 375–387.

Ulrich, R., Kral, T., Chevrier, V., Pilgrim, R., Roe, L., 2010. Dynamic temperature fields under mars landing sites and implications for supporting microbial life. Astrobiology 10, 643–650.

Zent, A.P., Haberle, R.M., Howard, C.H., Jakosky, B.M., 1993. A coupled subsurface-boundary layer model of water on Mars. J. Geophys. Res. 98, 3319–3337.

Zent, A.P. et al., 2010. Initial results from the thermal and electrical conductivity probe (TECP) on Phoenix. J. Geophys. Res. 115, E00E14.

Zent, A.P., Hecht, M.H., Hudson, T.L., Wood, S.E., Chevrier, V.F., 2012. A revised calibration function for the TECP humidity sensor of the Phoenix mission. Lunar Planet. Sci. XVIII. Abstract #2846.